Jet Engine Fan Blade Containment using Two Alternate Geometries

Authors:

Kelly Carney, Mike Pereira, Duane Revilock, and Paul Matheny*
NASA Glenn Research Center, Cleveland, Ohio
*Florida Turbine Technology**, West Palm Beach, Florida

Correspondence:

Kelly S. Carney
NASA Glenn Research Center
21000 Brookpark Rd.
Cleveland, Ohio 44135

Tel: (216) 433-2386
E-mail: Kelly.S.Carney@nasa.gov

Keywords:
Containment, fan case, impact, blade off, turbine engine, high strain rate material behavior

ABSTRACT

In the rare event of a fan blade separation, the fan blade must not penetrate the case of a commercial jet engine. Due to this requirement the fan case is the heaviest single component of a jet engine. With a goal of reducing that weight, a simulation of a fan blade containment system was tested at the NASA GRC Ballistic Impact Lab and analyzed using LS-DYNA. A fan blade simulating projectile was shot at two alternate geometric containment case configurations. The first configuration was a flat plate which represents a standard case configuration. The second configuration had a surface curved outward from the projectile. The curved surfaced forces the blade to deform plastically, dissipating energy before the full impact of the blade is received by the plate. The curved case was thus able to tolerate a higher velocity of impact before failure. The LS-DYNA analytical model was correlated to the tests and a weight savings assessment was performed.

INTRODUCTION

In order to insure passenger and crew safety, international aviation regulatory bodies, such as the Federal Aviation Administration in the United States and the Joint Aviation Authorities in Europe require that in commercial jet engines a system must exist which will not allow any compressor or turbine blade to perforate the engine case in the event that it is released from a disk during engine operation [3]. They further require that jet engine manufacturers demonstrate, through a certification test, that the most critical blade be contained within the engine when a blade is released while the engine is running at full rated thrust [1]. The most critical compressor blade in the engine, in terms of maximum kinetic energy, is invariably the fan blade, and the system designed to prevent it from penetrating the engine is called the fan containment system.

Figure 1 Uncontained Engine Failure

The fan containment system includes a cylindrical case which surrounds the fan blades and disk. In modern high bypass turbine engines the fan blades are large and, as a result, the fan cases contribute significantly to overall engine weight. There are two general types of fan containment systems, commonly referred to as hardwall and softwall systems. Hardwall systems consist of a relatively stiff section of the engine case that has sufficient strength to prevent perforation if impacted by a blade. Softwall systems usually consist of a relatively thin inner ring, surrounded by layers of dry fabric. Both systems include ribs and stiffeners which enhance system stiffness and both typically have flat cylindrical geometries. The geometry of the fan case can affect containment response. A careful selection of the geometry can improve containment and efficiency, allowing for case thickness reduction and reduced engine weight.

The loss of a fan blade in a high bypass turbine engine can be initiated by material failure due to fatigue, a bird strike [7], or some other foreign object damage. The fan blades are initially rotating at a very high rate, on the order of 5000 rpm. This large rotational kinetic energy determines both trajectory and resulting velocity of the released blade. The released blade will follow a tangential trajectory that is highly determined by these initial conditions. That trajectory will cause the blade to impact the containment case at a relatively consistent angle and orientation. The character of a blade off impact, including point of impact, is surprisingly repeatable for an event which is triggered randomly. As a result, the blade off event may be tested and designed for in a deterministic manner.

A case so designed for may, in the future, include a concatenated geometry with a shallow convex curve in the radial direction of the cylindrical case. As a released blade strikes the convex curve it will deform, converting its kinetic energy into plastic energy before the full weight of the blade impacts. The proposal that the convex curved geometry will aid in containment was preliminarily explored using LS-DYNA [4] analysis. After showing promise, a series of scaled tests was subsequently designed and performed, and the concept was verified. A final analysis was correlated with these tests, giving an estimate of the potential weight savings and yielding insight into the behavior of the subject materials at very high strain rates.
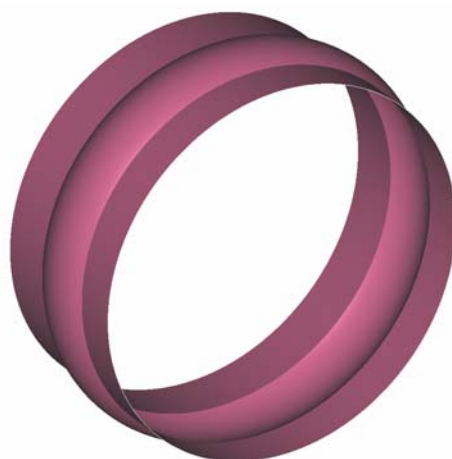

Figure 2
Convex Curve Fan
Case Geometry

Certain conditions must exist for the convex curved surface to be effective. The convex curve case requires sufficient strength and stiffness, relative to the blade, to maintain the curved geometry. Particularly, this includes system stiffness and local strength. System stiffness required to maintain the convex curved shape under impact, would normally be provided by ribs. A simulation of the rib stiffness was required in the test setup to successfully test this concept. The case must also be of sufficient thickness and strength to bend the tips of the incoming blade, without the local section being destroyed.

METHODS

Testing

The testing was conducted at the NASA Glenn Research Center Ballistic Impact Laboratory. The laboratory has a large gas gun consisting of a pressure vessel with a volume of 0.35 m^3 (12.5 ft^3), a gun barrel with a length of 12.2 m (40 ft) and an inner diameter of 20.32 cm (8.00 in). The pressure vessel and the gun barrel were mated by a flange on each side with a number of layers of Mylar® sheet sandwiched between the flanges to seal the pressure vessel and acting as a burst valve. Helium gas was used as the propellant. The pressurized helium was released into the gun barrel by applying a voltage across a Nichrome wire embedded in the Mylar sheets, causing the Mylar sheets to rupture. The projectile was supported by a wood block inside an aluminum can shaped cylindrical sabot that just fit inside the gun barrel. The sabot was stopped at the end of the gun barrel by a thick steel plate with a rectangular slot large enough to allow the projectile to pass through. The gun barrel was evacuated to reduce blast loading on the specimen and to reduce the amount of pressure needed to achieve the desired impact velocity.

Figure 3 Glenn Research Center Ballistic Impact Laboratory Gas Gun

For the test targets, the fan case is represented by 24.0 in by 24.0 in 304L stainless steel plates, with a thickness of 3/16 in. Half of the plates were flat and half had a shallow convex curve with a height of 5/6 in and a width of 5.0 in, as shown in Figure 4. The plates were securely clamped at their edges and two simple supports were placed on either side of the target, 8.0 in apart. The blades were simulated by a projectile made from Ti-6Al-4V titanium.

The blade simulating projectile was 5.0 in long, 3.8 in wide, and .2 in thick at the narrow end, and .5 in thick at the thick end, as shown in Figure 5. The plates were held at 45° in relation to the trajectory of the blade. The blade orientation was 45° in relation to its trajectory, opposite to that of the plate, as shown in Figure 6.

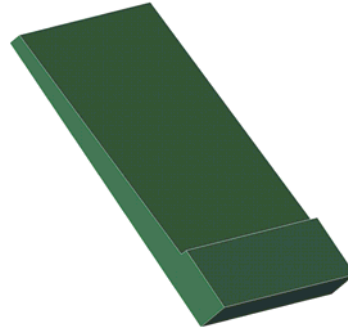**Figure 4** Target Plate with Convex Curve

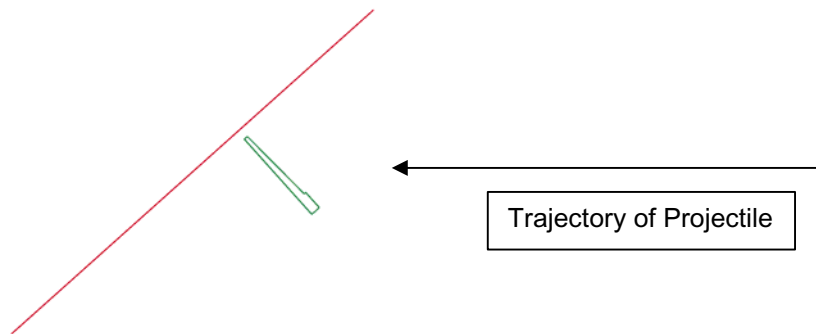**Figure 5** Blade Simulating Projectile

Trajectory of Projectile

Figure 6 Orientation of Impact

High speed digital video cameras (Phantom 5, Photosonics Inc., Burbank, CA) were used to record the position and orientation of the projectile during the experiment. The recording speed was 11200 frames per second, with a 256 x 256 pixel resolution. One camera was located at the side of the impact point and the other was at an oblique angle. For each test the position of the projectile was recorded as a function of time. The impact velocity was determined by fitting a straight line to the position data while in free flight and averaging the slopes of the resulting lines. In general, the projectile was obscured by the specimen during the impact itself, so it was not possible to obtain accurate enough position data to calculate the projectile deceleration and the resulting force on the projectile during the impact. After the test the plastic deformation and failure of both the target and the projectile was evaluated.

Analysis

The material model used for the 304L stainless steel plates was PLASTICITY WITH DAMAGE, type 81. This damage model successfully reproduced the tearing of steel which was observed in the ballistic tests. Several stress-strain curves defining the material behavior of 304L, at various strain rates, were used. The onset of damage was defined as .36 effective plastic strain, with failure occurring at .56 plastic strain. The static stress-strain curve, and the value of the onset of damage, was obtained by testing at Glenn Research Center. The high strain rate data used to create this model was obtained from Nicholas [6], and for very high strain rates, from Dowling [2].

The material model used for the Ti-6Al-4V titanium blade was PIECEWISE LINEAR PLASTICITY, type 24. Several stress-strain curves defining the material behavior of Ti-6Al-4V, at various strain rates, were used. Failure was defined at .22 effective plastic strain. The high strain rate data used to create this model was obtained from Nicholas [6] and Lesuer [5], and for very high strain rates, from Wulf [8].

The behavior of both the titanium and the stainless steel at strain rates greater than 5000 sec^{-1} was an important factor in directing the results of the complete system. Strain occurring at rates greater than approximately 5000 sec^{-1} yields region IV behavior. Below this rate, in region II, flow stress is proportional to logarithm of the strain rate. In region IV, the rate flow stress is directly proportional to the strain rate, resulting in much stronger material at these rates. It has been suggested [2] that at these high strain rates, the applied stress is sufficient for dislocation intersection to occur without the aid of thermal energy, so that the velocity of dislocations is governed by energy dissipation in the lattice itself. It very difficult to test at these strain rates, and as a result, it is also difficult to obtain data in region IV. As a result, the macroscopic viscosity (the slope of strain rate sensitivity) of the stainless steel [2] and the titanium from [8] was used to extend the strain rate curves into the untested strain rate values.
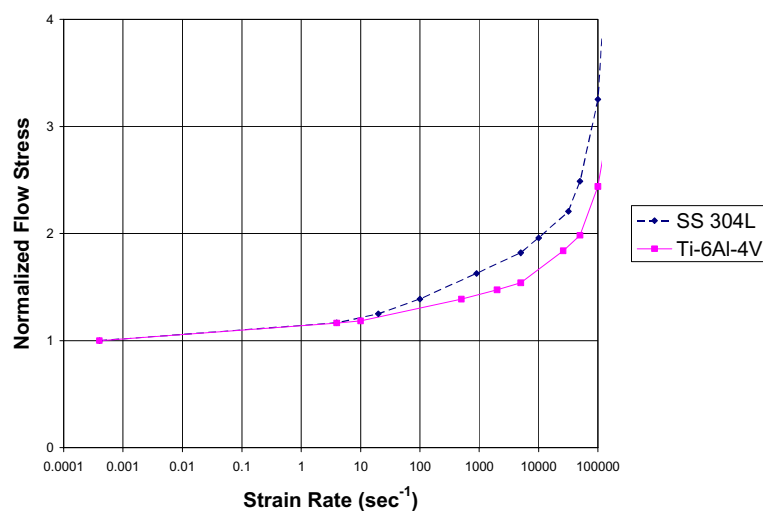

Figure 7 The Modeled Strain Rate Sensitivity of Ti-6Al-4V and SS-304L

The finite element model of the target plate consisted of 57,600 shell elements using the Belytschko-Tsay formulation. The dimensions of the shell elements were approximately .1 in by .1 in. The outside edges of the plates were clamp constrained and the 8 in wide simple supports, on either side of the impact area, were constrained only in the direction of impact. The blade was modeled with 6080 solid elements using the constant stress solid element. The dimensions of the solid elements were approximately .1 in by .1 in by .1 in.

RESULTS

The plates receive the initial strike from the blade projectile along an edge, which leaves an indentation in the plate. If the velocity of the projectile is high enough, the steel proceeds to tear catastrophically. At somewhat lower velocities, when the initial edge does not fail, the curve plates experience a perforation when the thick section of blade rotates into the plate, after initial impact. The curved plates are penetrated at about 1600 ft/sec and the flat plates are penetrated at about 1400 ft/sec. This observed advantage of approximately 200 ft/sec, which the convex curved plates have over the flat plates, is due to the energy that is absorbed by plastic deformation of the blade tips.

Figure 8 Flat Plate at 1300 ft/sec   **Figure 9** Flat Plate at 1400 ft/sec

Figure 10 Curved Plate at 1500 ft/sec   **Figure 11** Curved Plate at 1600 ft/sec

The analytical models were correlated to the test results by modifying the material models until the velocities and plastic strains at failure approximately matched. There were several indispensable modifications required to achieve this. The tearing failure in the plate was simulated by including a damage model to the stainless steel. The failure at .56 effective plastic strain for the steel, and .22 effective plastic strain to failure for the titanium, were found to reflect the ballistic test data. The unexpectedly high strength of both materials at the initial impact was achieved by defining their region IV, very high strain rate, behavior. LS-DYNA calculated strain rates on the order of 1.e6 sec^{-1} and so the high strain rate behavior was extrapolated up to 1.e7 sec^{-1} to insure a complete numerical definition.

After correlation, the LS-DYNA results generally match the ballistic tests with the following exceptions. In the analysis, the blade did not fragment into several pieces at higher velocities. This is due to the failure strain being set too high for the bending of the blade. However, if the failure strain is set lower, the initial impact causes much more damage to the blade than what was observed. This may be a problem with the failure model, but it could also be due to the great uncertainty in the high strain rate behavior of the titanium. The trajectory of the blade, after the initial impact, was somewhat too shallow causing the second impact to occur closer to the initial impact than what was observed in the test. There were also point failures in the plate at the 8 in wide simple supports. The actual supports were wider and did not allow the stress concentration that was produced by the mode.

Figure 12 Flat Plate 1300 ft/sec Analysis

Figure 13 Flat Plate 1400 ft/sec Analysis
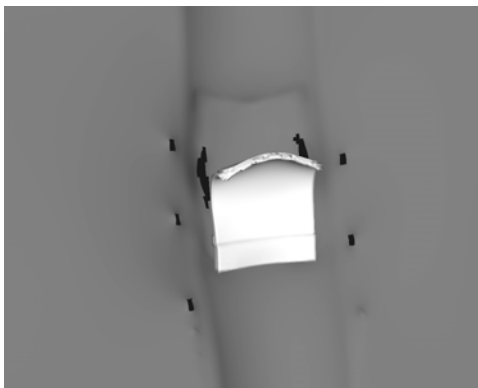

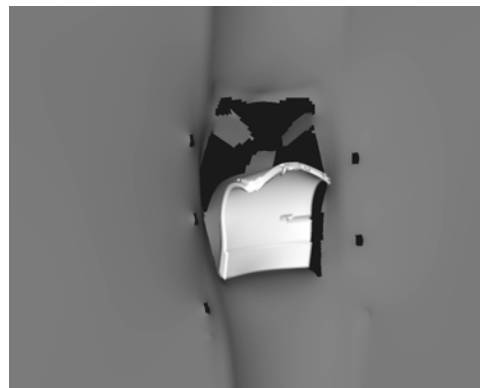**Figure 14** Curved Plate 1500 ft/sec Analysis

Figure 15 Curved Plate 1600 ft/sec Analysis

The convex curved design concept was evaluated by taking the correlated curve plate model, and reducing its thickness until the plate failed. This 1300 ft/sec velocity impact analysis was compared to the flat plate at the same velocity. The weight of the thinner convex curve section, taking into account its 7.25 % greater arc length, was compared to the 3/16 in thick flat plates. It was found that a curved section thickness of .15 in failed to the same degree as the flat plate baseline, yielding an approximate weight savings of 14% in the curved section of the concatenated fan case.

CONCLUSION

Using a fan case with convex curve geometry to increase containment efficiency has been demonstrated both by test and analysis. Both the test results and the correlated LS-DYNA model have shown a 200 ft/sec increase in containment capability using the curved geometry. A critical component of the correlation was the material behavior at strain rates greater than 5000 sec^{-1}. It is very difficult to test in the region, but for high speed impact analytical prediction capability to improve, this data must be sought.

REFERENCES

1. CARNEY, K.S., LAWRENCE, C., CARNEY, D.V. (2002) "Aircraft Engine Blade-Out Dynamics", 7ᵗʰ International LS-DYNA Users Conference.

2. DOWLING, A.R., HARDING, J., CAMPBELL, J.D. (1970) "The Dynamic Punching of Metals", J. Inst. Met. Vol. 98, pp. 215-224.

3. FEDERAL AVIATION ADMINISTRATION (1984) Federal Aviation Regulation Part 33, Section 33.94.

4. HALLQUIST, J.O., LIN, T., TSAY, C.S. (1993) "LS-DYNA Theoretical Manual", "Nonlinear dynamic analysis of solids in three dimensions", Livermore Software Technology Corp., Livermore.

5. LESUER, D.R. (2000) "Experimental Investigations of Material Models for Ti-6Al-4V Titanium and 2024-T3 Aluminum", DOT/FAA/AR-00/25.

6. NICHOLAS, T. (1980) "Dynamic Tensile Testing of Structural Materials Using a Split Hopkinson Bar Apparatus", AFWAL-TR-80_4053.

7. VASCO, T.J. (2000) "Fan Blade Bird-Strike Analysis and Design", 6ᵗʰ International LS-DYNA Users Conference.

8. WULF, G. L., (1979) "High-Strain Rate Compression of Titanium and Some Titanium Alloys", Int. J. Mech. Sci. Vol. 21, pp. 713-718.